IEEE Access
Multidisciplinary | Rapid Review | Open Access Journal

Received February 26, 2019, accepted April 7, 2019, date of publication April 12, 2019, date of current version April 26, 2019.

Digital Object Identifier 10.1109/ACCESS.2019.2911024

Fault-Tolerant Control of Double-Rope Winding Hoists Combining Neural-Based Adaptive Technique and Iterative Learning Method

XIAO CHEN, ZHEN-CAI ZHU, WEI LI, AND GANG SHEN

School of Mechatronic Engineering, China University of Mining and Technology, Xuzhou 221116, China
Jiangsu Key Laboratory of Mine Mechanical and Electrical Equipment, China University of Mining and Technology, Xuzhou 221116, China

Corresponding author: Zhen-Cai Zhu (zhuzhencai@cumt.edu.cn)

This work was supported in part by the National Natural Science Foundation of China under Grant U1810124, in part by the National Key Research and Development Program under Grant 2016YFC0600905, in part by the Program for Changjiang Scholars and Innovative Research Team in University under Grant IRT_16R68, and in part by the Priority Academic Program Development of Jiangsu Higher Education Institutions (PAPD).

ABSTRACT Double-rope winding mine hoist (DRWMH) is a vital coal mining equipment whose performance directly impacts the safe and efficient exploitation of the deep earth resources. Unfortunately, the actuator faults and disturbances can greatly affect the effect of the DRWMH. This paper deals with the problem of tension coordination control against actuator faults and disturbances for a DRWMH driven by multiple permanent magnet synchronous motors (PMSMs) using the neural-based adaptive method and iterative learning scheme. To improve the control performance and to maintain the stability of the DRWMH under faulty conditions, in this approach, a novel neural-based adaptive control strategy is developed to implement the input control assignment of the actuators. An iterative learning controller is used to achieve the compensation of the faults and uncertainties. The stability of both control subsystems has been proven. A series of experimental results are illustrated to demonstrate the validity of the proposed fault tolerant control for the DRWMH, which also reveal that a superior control effect is achieved in contrast with traditional controllers. Furthermore, the strategy proposed in this paper can be applied to other mechanical systems driven by multiple PMSMs that require high safety.

INDEX TERMS Double-rope winding mine hoist, fault-tolerant control, adaptive algorithm, iterative learning method, actuator failure, PMSM.

I. INTRODUCTION

Double-rope winding mine hoist (DRWMH), also known as Blair multi-rope system, is vital coal mining equipment whose performance directly impacts the safe and efficient exploitation of the deep earth resources. In the past few decades, with the rapid growth in energy consumption, researches on operation reliability of DRWMH have extensively increased [1]–[3]. Compared with the traditional single-rope winding hoists, DRWMH has the advantages of improved load capacity, lighter in weight, more cost-effective and safer performance since load on the conveyance can be shared by multiple cables. On the other hand, due to their complex coupled dynamics characteristic and the effect of disturbance, difficulty in control is still the major drawback associated with the DRWMH [4].

In fact, according to the practical experience of the past, the main factor limiting the use of the DRWMH is the broken rope which is mainly caused by the uneven tension of the ropes [5]. Therefore, the tension control of the ropes has attracted wide attention of scholars and forms an open field of research with the advancement of control theory research [6]. In the literature [7], a robust nonlinear adaptive back-stepping controller was used to adjust wire rope tensions for a double rope hoisting parallel. A nonlinear disturbance observer was applied to cope with the uncertainties. Reference [8] designed an output feedback boundary controller to solve the problem of tension oscillation inconformity in a dual-cable mining hoist. Reference [9] presented a type-2 fuzzy adaptive inverse controller for inclination and tension control

The associate editor coordinating the review of this manuscript and approving it for publication was Mark Kok Yew Ng.

of a cable-driven parallel system. Reference [10] proposed a robust PID controller for fully-constrained cable driven parallel manipulators with uncertain dynamic parameters. However, these studies focus on the suppression of system disturbances. When the actuators fail, the controller not only could not achieve the desired effect, but also would even cause serious safety accidents [11]. Therefore, a challenging problem for the DRWMH is how to ensure good performance of the controller when the actuator failure occurs.

Actually, in many practical safety-critical systems such as flight control system [12], satellite control system [13], and chemical control system [14], the design of the fault tolerant controller (FTC) has received a lot of attention and discussion. Several approaches have been proposed for stabilization of linear and nonlinear systems under actuator faults. In general, the existing FTC methods can be divided into two types: passive FTC and active FTC [15], [16]. For the passive FTC, the controller is directly designed robust enough to deal with faults and uncertainties. For instance, in the literature [17], a sliding mode control technique was used to design a robust controller for a quadrotor under actuator faults. Reference [18] presented a robust H_∞ controller with finite-frequency constraint for an active suspension system with actuator faults. However, passive FTC design must consider the type and size of the faults in advance, and can only deal with limited type of faults, which limits their use.

For the active FTC, the controller configures the control law online in real time based on fault or failure information, it usually necessitates a detection and identification (FDI) strategy to evaluate faults first. In [19], an actuator fault tolerant control scheme was proposed for differential-drive mobile robots based on the multiple-model approach. The linearized model and extended Kalman filter were used to detect, isolate and identify actuator faults. In the literature [20], the design problem of fault-tolerant dynamic surface controller for a class of uncertain nonlinear systems with actuator faults was discussed. Nonlinear adaptive fuzzy observers were constructed to estimate the actuator faults. A RBF neural network based fault estimation observer and a sliding mode based fault detection observer were designed to detect actuator faults for a rigid spacecraft in [21]. A fast terminal sliding mode control technique was further developed to compensate for faults.

In recent years, the number of researchers concentrating on solving the problem of fault tolerant controller design for linear and nonlinear systems using adaptive control method continues to increase [22], [23]. The direct adaptive fault tolerant control method does not require a fault detection and diagnosis (FDD) module or a quantitative parameter knowledge of the system, and thus is more suitable for industrial use. In [24], a model-free adaptive fault tolerant attitude tracking controller was developed for a flexible spacecraft in the presence of inertia uncertainties, external disturbances and uncertain actuator failures. A novel adaptive third-order sliding mode control based FTC strategy for permanent-magnet machines was presented in [25] where complicated fault detection and fault diagnosis algorithms can be avoided. In [26], a novel fault tolerant controller combing a backstepping technique and an adaptive method was proposed for a satellite under actuator faults.

As for the design of fault-tolerant controller for DRWMH, there are few theoretical results or experimental results. At the same time, hybrid factors consisting of drum winding interferences [27], flexible rope structure [28], friction at headgear sheave [29] and drive motor uncertainties [30] bring difficulties to the design of fault-tolerant controller. In this paper, a novel approach to design a robust adaptive controller is proposed to deal with actuator faults, where RBF neural network [31] is employed to handle actuator bias and uncertainties. Nevertheless, only relying on the function of closed-loop adaptive feedback still cannot effectively suppress the disturbance and completely eliminate the impact of the faults.

Thus, a feedforward feedback iterative learning controller (FFILC) is also presented to compensate uncertainties and remaining faults effects. As an intelligent control method, iterative learning controller (ILC) [32] is mainly used for disturbance suppression of complex systems with repetitive operation characteristics. Due to its simple design, ILC has been used in many applications to improve the control performance including robot manipulators [33], high-speed trains [34], batch processes [35], permanent-magnet machines [36] and cooperative multiple mobile cranes [37].

The main contribution of this research is to present a novel hybrid controller utilizing both adaptive method and iterative learning strategy to deal with uncertainties and actuator faults for a form of DRWMH driven by permanent magnet synchronous motors (PMSM), and its verification in a DRWMH experimental platform. The stability of overall controllers in presence of actuator faults and uncertainties is proven. To verify the effectiveness of the proposed algorithm, a number of comparative experimental studies have been conducted on a DRWMH test platform under different actuator faults working conditions. The experimental results show that the proposed method has better fault tolerance performance than traditional PID controller and FFILC.

The rest of the paper is organized as follows. The structure of DRWMH and the configuration of the test bench are described in the following section. Section 3 presents dynamics model of the mechanical subsystem and electrical model of the PMSM. Specific design details and stability proof of the proposed controller are discussed in Section 4. Section 5 demonstrates a series of comparative experimental results and analyzes the performance of the three algorithms under different working conditions. Section 6 draws conclusions.

II. SYSTEM STRUCTURE AND TEST PLATFORM

A. STRUCTURE OF THE DOUBLE-ROPE WINDING MINE HOIST

The double-rope winding mine hoist can be divided into two parts with the same structure, as shown in Figure 1. Each part consists of two wire ropes wound on the same winder

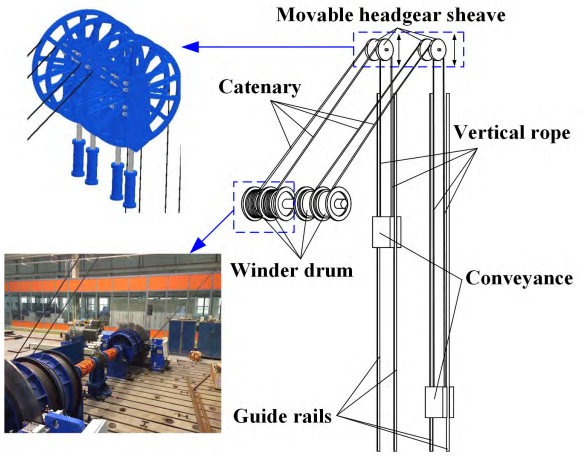

FIGURE 1. Double-rope winding mine hoist.

drum, two movable headgear sheaves fixed above the tower, and a conveyance suspended at both ends of the ropes. When the motor drives the winder drum to wind the wire ropes, the force is transmitted to the conveyance along the wire ropes, and the conveyance is moved up and down. One side of the conveyance rises while the other side of the conveyance descends, thereby achieving continuous coal transportation. In the actual operation process, the unavoidable factors such as rope groove deviation and stiffness deviation will cause the deviation of the rope length and lead to the tension imbalance. At this time, the movable headgear sheaves move up and down to adjust the rope length so that tension inconformity between wire ropes can be eliminated. However, in the event of a movable headgear sheave fails, it will be difficult for the controller to achieve inherent regulation performance, posing a potential risk to the safe operation of the system.

B. STRUCTURE OF THE TEST PLATFORM

Taking into account the damage that may be caused by the failure experiment, in this section, a small experimental system is built to simulate the actual working conditions of DRWMH and test the controller's effect. Figure 2 illustrates the structure diagram of the experimental DRWMH platform driven by PMSMs. The experimental platform mainly comprises eight components: a winding drum driven by PMSM (PMSM-1), two hoisting ropes, two movable headgear sheaves driven by PMSMs (PMSM-2 and PMSM-3), two guide rails fixed to the ground, a conveyance, a host computer, a real-time control system and two tension sensors.

The PMSMs use the same model, whose specifications are as follows: rated output power 400 W, maximum rotation speed 3000 rpm, and rated torque 1.3 Nm. Each motor comes with an encoder that can measure real-time speed and is connected to a reducer whose reduction ratio is 10 to increase output torque. The tension sensors which are configured with a range of 0-200 N and an output of 0-5V are mounted at the connection of the ropes and the conveyance.

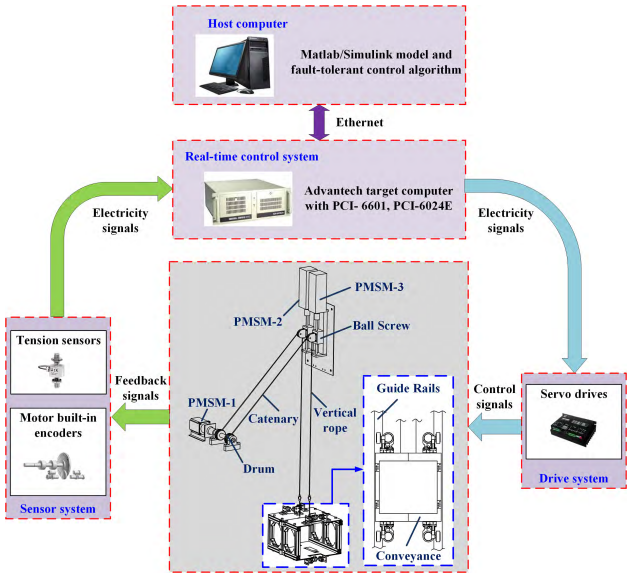

FIGURE 2. The real-time experimental system of DRWMH.

The real-time control system consists of an IPC-610-L Advantech target computer and several boards installed in it. The No. 1 PMSM is implemented by the PCI-6024E board, which can measure the rope tensions at the same time. The control style of No. 2 and No. 3 PMSM adopts the sine-wave pulse-width modulation (PWM) from PCI-6601 board. The role of the host computer is to edit and compile control strategy related code under Matlab/Simulink environment, and then sending the codes to target computer for real-time running. The target computer collects sensor signals and calculates the output signals for real-time control. The sampling interval of the control system has been set as 1000Hz.

III. MATHEMATICAL MODEL OF DRWMH

In this section, for subsequent analysis and controller design, the mathematical model of DRWMH mechanical subsystem is given, and the electrical equation of the PMSM is formulated.

A. MATHEMATICAL MODEL OF THE MECHANICAL SUBSYSTEM

Figure 3(a) shows the multi-degree-of-freedom dynamic model of the mechanical subsystem, in which the rope characteristics are described by the mass-spring-damping model. Figure 3(b) is the equivalent dynamic model of the movable headgear sheave.

According to DRWMH dynamics theory, the motion equations of connection sites are [38]

$$m_{vri}\ddot{d}_{vri} - (\theta_{si}r_{si} + d_{si} - d_{vri})\,k_{vi} + F_{vri} - \left(\dot{\theta}_{si}r_{si} + \dot{d}_{si} - \dot{d}_{vri}\right)c_{vi} = 0, \quad i = 1, 2 \quad (1)$$

where $m_{vri}(i = 1, 2)$ represent the mass of the connection sites. $d_{vri}(i = 1, 2)$ indicate the longitudinal displacements of the connection site. The angular displacements and equivalent radius of the headgear sheaves are denoted by $\theta_{si}(i = 1, 2)$

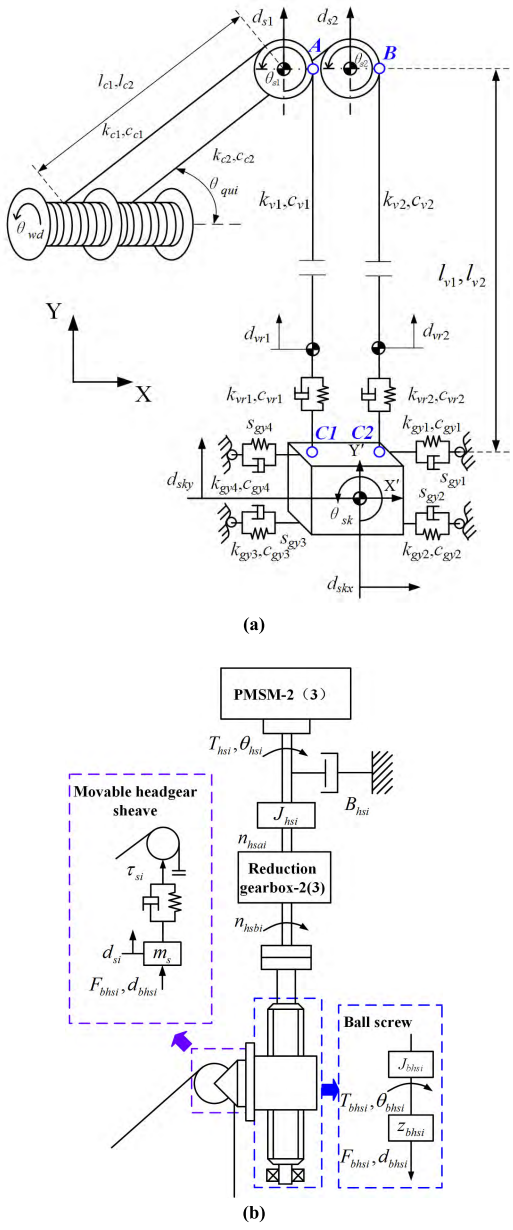

FIGURE 3. Mathematical model of the mechanical subsystem of DRWMH. (a) Equivalent dynamic model of the hoisting subsystem (b) Equivalent dynamic model of the movable headgear sheave.

and $r_{si}(i = 1, 2)$. The longitudinal displacements of the two movable headgear sheaves are denoted by $d_{si}(i = 1, 2)$. $d_{vri}(i = 1, 2)$ indicate the longitudinal displacements of the connection site. $k_{vi}(i = 1, 2)$, $c_{vri}(i = 1, 2)$ are the equivalent stiffness coefficient and equivalent damping coefficient of the vertical ropes, respectively. F_{vr1} and F_{vr2} indicate force at the left connection site and the right connection site.

As shown in Figure 3(a), the conveyance is a three-degrees-freedom system whose mathematical model can be described by equations as follows

$$m_{sk}\ddot{d}_{skx} + \sum_{i=1}^{4}\left(k_{gyi}s_{gyi} + c_{gyi}\dot{s}_{gyi}\right) - \left(\sum_{i=1}^{2} F_{vri}\sin\theta_{vri}\right) = 0 \tag{2}$$

$$m_{sk}\ddot{d}_{sky} - \left(\sum_{i=1}^{2} F_{vri}\cos\theta_{vri}\right) = 0 \tag{3}$$

$$J_{sk}\ddot{\theta}_{sk} - p_{gy}\left(\theta_{sk}, \dot{\theta}_{sk}\right) + T_l + T_h = 0 \tag{4}$$

where the inertia and the mass of the conveyance are denoted by J_{sk} and m_{sk}, respectively.

The overall impact moment of force on conveyance is

$$p_{gy}\left(\theta_{sk}, \dot{\theta}_{sk}\right) = \sum_{i=1}^{4}\left(k_{gyi}s_{gyi}y_{gyi} + c_{gyi}\dot{s}_{gyi}y_{gyi}\right) \tag{5}$$

where the local frame vertical coordinates of four guide shoes are denoted by $y_{gyi}(i = 1, 2, 3, 4)$. The equivalent stiffness coefficient, equivalent damping coefficient and displacement change in the horizontal direction of the guide shoes are represented by $k_{gyi}(i = 1, 2, 3, 4)$, $c_{gyi}(i = 1, 2, 3, 4)$ and $s_{gyi}(i = 1, 2, 3, 4)$, respectively.

The moment of action of the longitudinal component of the rope force on the conveyance is denoted by

$$T_l = F_{vr1}\cos\theta_{vr1}r_{xc1} - F_{vr2}\cos\theta_{vr2}r_{xc2} \tag{6}$$

where θ_{vr1} and θ_{vr2} indicate swing angles of vertical ropes in the left side and vertical ropes in the right side, respectively. The transverse distance from conveyance centroid to the left connector point and the right points are stated by r_{xc1} and r_{xc2}.

The moment of action of the horizontal component of the rope force on the conveyance can be given as

$$T_h = \sum_{i=1}^{2} F_{vri}\sin\theta_{vri}r_{yci} \tag{7}$$

The vertical distance from conveyance centroid to the left connector point and the right points are expressed by r_{yc1} and r_{yc2}, respectively.

B. MATHEMATICAL MODEL OF THE PMSM

Since the motors used in the experiment platform are PMSMs, assuming that the motors are fed by balanced voltages and that the motors are symmetrical, the mathematical model of the motors in the dq reference frame can be described as follows [39]

$$u_d = Ri_d + L_d\frac{d}{dt}i_d - \omega_e L_q i_q \tag{8}$$

$$u_q = Ri_q + L_q\frac{d}{dt}i_q + \omega_e\left(L_d i_d + \psi_f\right) \tag{9}$$

where ω_e denotes the electric angle speed. The stator voltages along the d and q are represented by u_d and u_q. L_d and L_q indicate inductance along the d and q axes, respectively. The current along the d and q are denoted by i_d and i_q. ψ_f represents the magnet flux linkage, and the number of motor pole pair is denoted by p_n.

As the selected PMSMs are surface-mounted, it can be assumed that L_d is equal to L_q. The electromagnetic torque model of the driving motors can be expressed as follows

$$T_e = \frac{3}{2}p_n i_q\left[i_d\left(L_d - L_q\right) + \psi_f\right] = \frac{3}{2}p_n i_q\psi_f = Z_{pm}i_q \tag{10}$$

where $Z_{pm} = \frac{3}{2}p_n\psi_f$ indicates the input coefficient of the driving motors.

IV. FAULT TOLERANT CONTROL STRATEGY

This section illustrates a hybrid adaptive learning strategy for fault tolerant control of the DRWMH with actuator faults and disturbances. The simplified closed-loop control diagram can be seen in Figure 4. Main features of the proposed fault tolerant controller are: (1) an adaptive law is designed to deal with the movable headgear sheave faults, whose parameters are calculated in real time under the condition of Lyapunov stability; and (2) introducing feedback-feedforward iterative learning controller (FFILC) to handle uncertainties and excessive fault error.

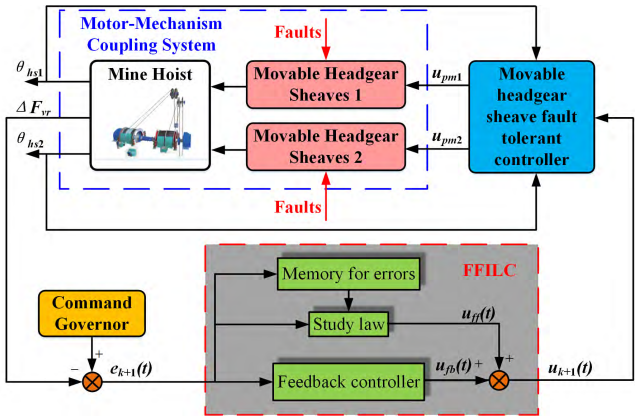

FIGURE 4. Simplified closed-loop control diagram.

A. CONTROLLER FOR THE MOVABLE HEADGEAR SHEAVE SUBSYSTEM

According to Equations (8)-(10), based on the rotor field orientation control method ($i_d = 0$), the mathematical model of PMSM can be described as

$$\begin{cases} \dfrac{d}{dt}i_{qj} = -\dfrac{Ri_{qj}}{L_q} - \dfrac{\omega_{ej}\psi_f}{L_q} + \dfrac{u_{qj}}{L_q} \\ \dfrac{d}{dt}\omega_{hsj} = \dfrac{1}{J_{pm}}\left(Z_{pm}i_{qj} - B_{hs}\omega_{hsj} - \tau_{sj}\right) \quad (j = 1, 2) \end{cases} \tag{11}$$

where inertia, speed damping coefficient and load variable of the motors are denoted by J_{pm}, B_{hs} and $\tau_{sj}(j = 1, 2)$.

State variable of the PMSM can be defined as $\boldsymbol{q}_{pm} = \left[\, q_{pm1}\ q_{pm2} \,\right]^T = \left[\, \theta_{hs1} - \theta_{hs2} \quad \omega_{hs1} - \omega_{hs2} \,\right]^T$. Input variable of the motor is defined as $u_{pmj} = i_{qj}$ $(j = 1, 2)$.The state space equation of the PMSM can be given as

$$\begin{cases} \dot{q}_{pm1} = q_{pm2} \\ \dot{q}_{pm2} = \dfrac{1}{J_{pm}}\left(Z_{pm}\left(u_{pm1} - u_{pm2}\right) - B_{hs}q_{pm2} - \tau_{s1} + \tau_{s2}\right) \end{cases} \tag{12}$$

The angular error and its change rate can be defined as

$$\begin{cases} e_{pm} = \theta_{hsr} - (\theta_{hs1} - \theta_{hs2}) \\ \dot{e}_{pm} = \dot{\theta}_{hsr} - \left(\dot{\theta}_{hs1} - \dot{\theta}_{hs2}\right) \\ e_{pm1} = \theta_{hsr}/2 - \theta_{hs1} \\ \dot{e}_{pm1} = \dot{\theta}_{hsr}/2 - \dot{\theta}_{hs1} \\ e_{pm2} = \theta_{hsr}/2 + \theta_{hs2} \\ \dot{e}_{pm2} = \dot{\theta}_{hsr}/2 + \dot{\theta}_{hs2} \end{cases} \tag{13}$$

where θ_{hsr} is the reference angular of the PMSM.

Consider the following faults form of the headgear sheave actuators

$$\begin{cases} u_{pm1} = \beta_{pm1}u_{pmo1} + u_{\xi 1} \\ u_{pm2} = \beta_{pm2}u_{pmo2} + u_{\xi 2} \end{cases} \tag{14}$$

where β_{pm1} and β_{pm2} are the performance loss factors of the left movable headgear sheave and the right movable headgear sheave. $u_{\xi 1}$ and $u_{\xi 2}$ are actuator bias of the left movable headgear sheave and the right movable headgear sheave. Depending on different values of $\beta_{pmi}(i = 1, 2)$ and $u_{\xi i}(i = 1, 2)$, different actuator fault forms can be expressed, as shown in Figure 5, where $p_{\max}$ and $p_{\min}$ represent maximum position and minimum position of the actuator respectively. For instance, assuming that the fault occurs at $t = 0.6$ s, if $\beta_{pmi} = 0$ and $u_{\xi i} = 0$, the corresponding actuator occurs lock-in-place fault, if $0 < \beta_{pmi} < 1$ and $u_{\xi i} = 0$, the corresponding actuator occurs loss of effectiveness fault, if $\beta_{pmi} = 1$ and $u_{\xi i} \neq 0$, the corresponding actuator occurs random fluctuation fault.

Assumption 1: Since the neural network has a universal approximation, in this paper, it is assumed that the actuator bias difference can be approximated as follows

$$u_{\xi 2} - u_{\xi 1} = \boldsymbol{\varphi}_{pm}^T\boldsymbol{R}_{pm}(x) + \varsigma_{pm} \tag{15}$$

where $\boldsymbol{\varphi}_{pm} = \left[\, \varphi_1\ \varphi_2\ \ldots\ \varphi_m \,\right]^T$ indicates the ideal approximation weight vector of the actuator bias difference. $\boldsymbol{R}_{pm} = \left[\, r_1\ r_2\ \ldots\ r_m \,\right]^T$ represents the ideal approximation radial basis vector. The approximation error is denoted by ς_{pm}, which is assumed to be bounded and satisfy $\left|\varsigma_{pm}\right| < \varsigma_{pmb}$. The Gaussian function is chosen as the activation function. Each neuron output of the hidden layer can be obtained as

$$r_j(x) = \exp\left(-\frac{\left\|\boldsymbol{x} - \boldsymbol{o}_j\right\|^2}{2h_j^2}\right) \quad j = 1, 2, \ldots m \tag{16}$$

where $r_j(x)$ is the ideal radial basis variable. $x = [x_1\ x_2\ \ldots\ x_n]^T$ indicates the input vector. $o_j = \left[o_{j1}\ o_{j2}\ \ldots\ o_{jn}\right]^T$ is center vector of the j-th node. h_j represents the base width variable.

Define the following error function as

$$s_{pm}(t) = J_{pm}\dot{\theta}_{hsr}(t) - \int_0^t \left(J_{pm}\left(\ddot{\theta}_{hs1} - \ddot{\theta}_{hs2}\right)\right)dt + \int_0^t \left(\kappa_{pm}\dot{e}_{pm}(t) + \gamma_{pm}e_{pm}(t)\right)dt \tag{17}$$

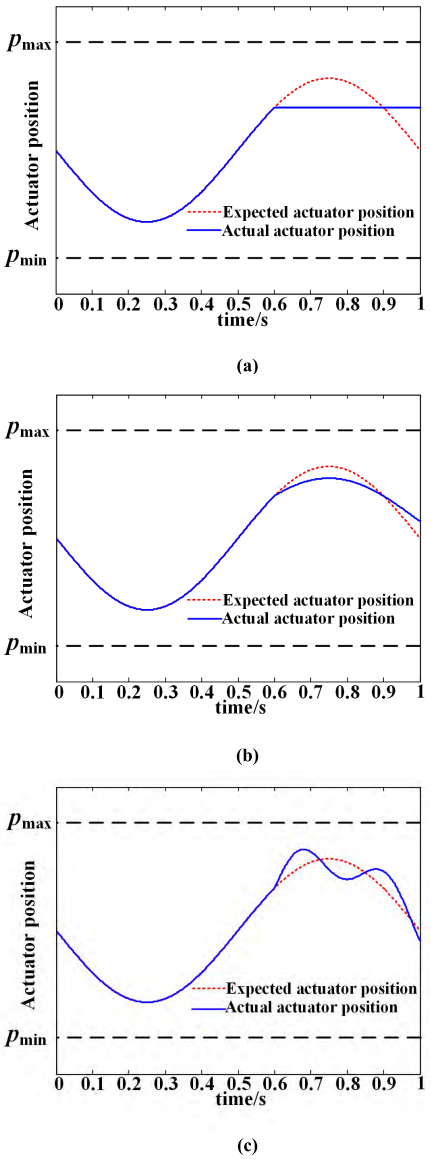

FIGURE 5. Type of actuator faults: (a) Lock-in-place; (b) Loss of effectiveness; (c) Random fluctuation.

From Equation (12) and (17), the derivative of the error function can be obtained as follows

$$\dot{s}_{pm}(t) = -\left(Z_{pm}\left(u_{pm1}-u_{pm2}\right)-B_{hs}q_{pm2}-\tau_{s1}+\tau_{s2}\right) + \kappa_{pm}\dot{e}_{pm}(t)+\gamma_{pm}e_{pm}(t)+J_{pm}\ddot{\theta}_{hsr}(t) \quad (18)$$

The current adaptive control law can be designed by

$$\begin{cases} u_{pmo1} = \tilde{\chi}_{pm1}\iota_{pm1} \\ u_{pmo2} = -\tilde{\chi}_{pm2}\iota_{pm2} \end{cases} \quad (19)$$

where

$$\iota_{pm1} = \frac{\varpi_{pm}s_{pm}}{2}+\frac{J_{pm}\ddot{\theta}_{hsr}(t)}{2}+B_{hs}\omega_{hs1}+\tau_{s1}+\frac{\kappa_{pm}\dot{e}_{pm1}(t)}{2} + \frac{\gamma_{pm}e_{pm1}(t)}{2}+\frac{Z_{pm}\hat{\boldsymbol{\varphi}}_{pm}^{T}\boldsymbol{R}_{pm}(x)}{2}+\frac{\lambda_{pm}\mathrm{sgn}(s_{pm})}{2} \quad (20)$$

$$\iota_{pm2} = \frac{\varpi_{pm}s_{pm}}{2}+\frac{J_{pm}\ddot{\theta}_{hsr}(t)}{2}-B_{hs}\omega_{hs2}-\tau_{s2}+\frac{\kappa_{pm}\dot{e}_{pm2}(t)}{2} + \frac{\gamma_{pm}e_{pm2}(t)}{2}+\frac{Z_{pm}\hat{\boldsymbol{\varphi}}_{pm}^{T}\boldsymbol{R}_{pm}(x)}{2}+\frac{\lambda_{pm}\mathrm{sgn}(s_{pm})}{2} \quad (21)$$

$\varpi_{pm}, \kappa_{pm}, \gamma_{pm}, \lambda_{pm}$ are four positive constants.

Let adaption laws to be defined as follows

$$\begin{aligned} \dot{\hat{\chi}}_{pm1} &= \mu_{pm1}s_{pm}\iota_{pm1}\mathrm{sgn}\left(\nu_{pm1}\right), \\ \dot{\hat{\chi}}_{pm2} &= \mu_{pm2}s_{pm}\iota_{pm2}\mathrm{sgn}\left(\nu_{pm2}\right), \\ \dot{\hat{\boldsymbol{\varphi}}}_{pm} &= Z_{pm}\eta_{pm}s_{pm}\boldsymbol{R}_{pm}(x). \end{aligned} \quad (22)$$

Theorem 1: For the driving motor mathematical equation described by Equation (12), if the adaptive control law (19) is applied, then the final state error is bounded.

Proof: Design a Lyapunov function as follows

$$V_{pm}(t) = \frac{1}{2}s_{pm}^{2}+\frac{|\nu_{pm1}|}{2\mu_{pm1}}\hat{\chi}_{pm1}^{2}+\frac{|\nu_{pm2}|}{2\mu_{pm2}}\hat{\chi}_{pm2}^{2} + \frac{1}{2\eta_{pm}}\tilde{\boldsymbol{\varphi}}_{pm}^{T}\tilde{\boldsymbol{\varphi}}_{pm} \quad (23)$$

where $\nu_{pm1} = Z_{pm}\beta_{pm1}$, $\nu_{pm2} = Z_{pm}\beta_{pm2}$. $\hat{\chi}_{pm1} = \tilde{\chi}_{pm1} - \chi_{pm1}$, $\hat{\chi}_{pm2} = \tilde{\chi}_{pm2} - \chi_{pm2}$, $\tilde{\boldsymbol{\varphi}}_{pm} = \hat{\boldsymbol{\varphi}}_{pm} - \boldsymbol{\varphi}_{pm}$ are three adaptive parameters. χ_{pmi} satisfies $\chi_{pmi} = 1/\nu_{pmi} (i = 1, 2)$.

The derivative of Lyapunov function with time is given as

$$\dot{V}_{pm}(t) = s_{pm}\dot{s}_{pm}+\frac{|\nu_{pm1}|}{\mu_{pm1}}\hat{\chi}_{pm1}\dot{\hat{\chi}}_{pm1}+\frac{|\nu_{pm2}|}{\mu_{pm2}}\hat{\chi}_{pm2}\dot{\hat{\chi}}_{pm2} + \frac{1}{\eta_{pm}}\tilde{\boldsymbol{\varphi}}_{pm}^{T}\dot{\hat{\boldsymbol{\varphi}}}_{pm} \quad (24)$$

Using (14) and (19), we can write (24) as follows

$$\begin{aligned} \dot{V}_{pm}(t) &= s_{pm}\left(-Z_{pm}\beta_{pm1}\tilde{\chi}_{pm1}\iota_{pm1}-Z_{pm}\beta_{pm2}\tilde{\chi}_{pm2}\iota_{pm2}\right) \\ &\quad + s_{pm}\left(B_{hs}q_{pm2}+\tau_{s1}-\tau_{s2}-Z_{pm}u_{\xi1}+Z_{pm}u_{\xi2}\right) \\ &\quad + s_{pm}\left(\kappa_{pm}\dot{e}_{pm}(t)+\gamma_{pm}e_{pm}(t)\right)+\nu_{pm1}\hat{\chi}_{pm1}s_{pm}\iota_{pm1} \\ &\quad + \nu_{pm2}\hat{\chi}_{pm2}s_{pm}\iota_{pm2}+Z_{pm}\tilde{\boldsymbol{\varphi}}_{pm}^{T}s_{pm}\boldsymbol{R}_{pm}(x) \\ &\quad + s_{pm}J_{pm}\ddot{\theta}_{hsr}(t) \end{aligned} \quad (25)$$

Introducing (20) and (21), it is clear that

$$\begin{aligned} \dot{V}_{pm}(t) &= s_{pm}\left(-Z_{pm}\hat{\boldsymbol{\varphi}}_{pm}^{T}\boldsymbol{R}_{pm}(x)-\lambda_{pm}\mathrm{sgn}(s_{pm})\right) \\ &\quad -\varpi_{pm}\left(s_{pm}\right)^{2}+Z_{pm}s_{pm}\left(\boldsymbol{\varphi}_{pm}^{T}\boldsymbol{R}_{pm}(x)+\varsigma_{pm}\right) \\ &\quad + Z_{pm}\tilde{\boldsymbol{\varphi}}_{pm}^{T}s_{pm}\boldsymbol{R}_{pm}(x) \end{aligned} \quad (26)$$

It is obvious that

$$\dot{V}_{pm}(t) = -\varpi_{pm}\left(s_{pm}\right)^{2}+s_{pm}\left(Z_{pm}\varsigma_{pm}-\lambda_{pm}\mathrm{sgn}(s_{pm})\right) \quad (27)$$

Then we further obtain

$$\dot{V}_{pm}(t) \le Z_{pm}\varsigma_{pmb}\left|s_{pm}\right|-\lambda_{pm}s_{pm}\mathrm{sgn}(s_{pm}) \quad (28)$$

Therefore $\dot{V}(t)$ becomes

$$\dot{V}_{pm}(t) \leq \left(Z_{pm}\varsigma_{pmb} - \lambda_{pm}\right)\left|s_{pm}\right| \tag{29}$$

Take $\lambda_{pm} \geq Z_{pm}\varsigma_{pmb}$, hence

$$\dot{V}_{pm}(t) \leq \left(Z_{pm}\varsigma_{pmb} - \lambda_{pm}\right)\left|s_{pm}\right| \leq 0 \tag{30}$$

Integrating (30) from 0 to t we can get

$$V_{pm}(0) \geq V_{pm}(t) + \int_0^t \vartheta_{pm}(\tau)d\tau \tag{31}$$

where $\vartheta_{pm}(\tau) = -\left|s_{pm}\right|\left(Z_{pm}\varsigma_{pmb} - \lambda_{pm}\right)$.

And then we can get

$$\dot{V}_{pm}(t) \leq 0, \quad V_{pm}(0) - V_{pm}(t) \geq 0 \tag{32}$$

which means that V is bounded, and s_{pm}, χ_{pm1}, χ_{pm2} are all bounded. Therefore, stability of the movable headgear sheave fault tolerant controller is ensured.

B. CONTROLLER FOR HOISTING SUBSYSTEM

The mathematical model of the mechanical subsystem described by Equations (1)-(4) is too complicated to design the controller. However, in the actual working conditions, due to the limitation of the guide rails, the swing angles of the vertical ropes are very small and can be neglected, which means that $\theta_{vr1} = \theta_{vr2} \approx 0$. In the meantime, except for the length, the remaining parameters of the ropes on both sides can be considered the same. Under above conditions, take the input of the hoisting subsystem as $u_c = \theta_{hsr1}$ - θ_{hsr2}, where θ_{hsr1} = - $\theta_{hsr2} = \theta_{hsr}/2$. From Equations (1) and (4), the simplified state space equation of the hoisting subsystem can be obtained as

$$M_{sk}\ddot{\theta}_{sk} - P_{sk}\left(\theta_{sk}, \dot{\theta}_{sk}\right) - d_{sk} = G_{sk}u_{sk} \tag{33}$$

where

$$M_{sk} = \frac{J_{sk}}{r_{xc}}, \quad P_{sk}\left(\theta_{sk}, \dot{\theta}_{sk}\right) = \frac{p_{gy}\left(\theta_{sk}, \dot{\theta}_{sk}\right)}{r_{xc}}, \quad G_{sk} = \frac{k_v}{z_{bhs}i_{hs}}.$$

Here, the drive ratio of gear speed reducer is denoted by $i_{hs} = i_{hsj}(j = 1, 2)$. The drive ratio of the ball screw is stated by $z_{bhs} = z_{bhsi}(i = 1, 2)$. The equivalent stiffness coefficient of the both vertical ropes can be represented by $k_v = k_{vi}(i = 1, 2)$. $c_v = c_{vi}(i = 1, 2)$ denotes the equivalent viscous coefficient of the both vertical ropes. The transverse distance from conveyance centroid to the connector points can be denoted by $r_{xc} = r_{xci}(i = 1, 2)$. The unmodeled state, model mismatch, disturbances and actuator faults are all denoted by $d_{sk}(t)$. $u_{sk}(t)$ represents the input of the hoisting subsystem.

Since the signals measured by the sensors are the end tensions of the two wire ropes. The output equation of the hoisting subsystem can be obtained as

$$y_c = \Delta F_{vr}^k = \rho_{sk}\theta_{sk} \tag{34}$$

where $\Delta F_{vr} = F_{vr1} - F_{vr2}$ represents the calculated tension difference. The measurement coefficient is denoted by ρ_{sk}.

Remark 1: For the actual DRWMH, the following two properties hold.

(P1) In each condition, the initial resetting condition meet $\left\|x_d(0) - x_c^k(0)\right\| \leq g_{x0}$.

(P2) The sum of model mismatch and uncertainties are bounded and meet $\|d_{sk}\| \leq g_d$.

The output of the designed FFILC can be obtained as

$$u_{sk}(t) = u_{fb}(t) + u_{ff}(t) \tag{35}$$

where the feedback part of the controller is denoted by $u_{fb}(t)$ and the feedforward part is indicated by $u_{ff}(t)$,respectively.

$$u_{fb}(t) = K_{skp1}e_{skf}^{k+1}(t) + K_{ski1}\int_0^t e_{skf}^{k+1}(\tau)d\tau + K_{skd1}\dot{e}_{skf}^{k+1}(t) \tag{36}$$

$$u_{ff}(t) = K_{skd2}\left(\varpi_{sk}e_{skf}^k(t) + \dot{e}_{skf}^k(t)\right) + u_{ff}(t - T) \tag{37}$$

where $e_{skf}^k(t) = \Delta F_{vrd}^k(t) - \Delta F_{vr}^k(t)$ represents the error between the desired tension difference and the measured tension difference in the process of kth operation, the derivative of which is denoted by $\dot{e}_{skf}^k(t)$. T is the cycle time of an iteration and$\varpi_{sk} = K_{skp2}/K_{skd2}$.

Along desired conveyance rotation angle $(\theta_{dsk}, \dot{\theta}_{dsk})$, (33) can be linearized according to Taylor formula as [40]

$$M_{sk}\ddot{e}_{sk}^{k+1} + C_{sk}\left(\dot{e}_{sk}^{k+1}\right) + F_{sk}\left(e_{sk}^{k+1}\right) = \eta_{skd} - M_{sk}\ddot{\theta}_{sk} + P_{sk}\left(\theta_{sk}, \dot{\theta}_{sk}\right) + O_{p_{gy}}(\bullet) \tag{38}$$

where

$$C_{sk} = -\left.\frac{\partial P_{sk}}{\partial \dot{\theta}_{sk}}\right|_{\theta_{dsk}, \dot{\theta}_{dsk}}, F_{sk} = -\left.\frac{\partial P_{sk}}{\partial \theta_{sk}}\right|_{\theta_{dsk}, \dot{\theta}_{dsk}}$$

$$\eta_{skd} = M_{sk}\ddot{\theta}_{dsk} - P_{sk}\left(\theta_{dsk}, \dot{\theta}_{dsk}\right)$$

Theorem 2: For the nonlinear hoisting subsystem (33), if the feedback feedforward iterative control law (35) is adopted, then both the error of the tension difference and the error of the final state are bounded, with the control gains meet following inequalities.

$$\sqrt{\phi_{ska}\phi_{skb}} > \frac{1}{\sqrt{\varpi_{sk}}}\left(\varpi_{sk}\phi_{ska} + \frac{1}{2}\zeta_{sk}\right) \tag{39}$$

where

$$\phi_{ska} = \rho_{sk}G_{sk}K_{skd1} - \frac{\rho_{sk}G_{sk}K_{skd2}}{2} - \varpi_{sk}M_{sk} - \gamma_{csk} > 0 \tag{40}$$

$$\phi_{skb} = \rho_{sk}G_{sk}K_{skp1} - \frac{\rho_{sk}G_{sk}K_{ski1}}{\varpi_{sk}} - \frac{G_{sk}K_{skd2}\varpi_{sk}}{2} - \zeta_{sk} > 0 \tag{41}$$

$$\zeta_{sk} = \max_{t\in[0,t]}\left\{2\varpi_{sk}\|C_{sk}\| + \|F_{sk}\|\right\}, \quad \gamma_{csk} = |C_{sk}| \tag{42}$$

Proof: Please see Appendix.

Remark 2: Since the mixing errors in the actual subsystem cannot be avoided, both the error of the tension difference and the error of final state cannot converge to zero.

V. RESULTS AND DISCUSSION

To assess the effect of the proposed hybrid fault tolerant controller, a set of experiments have been performed on the test bench described in Section 2. The photograph of the bench is presented in Figure 6, and its specifications are listed in Table 1.

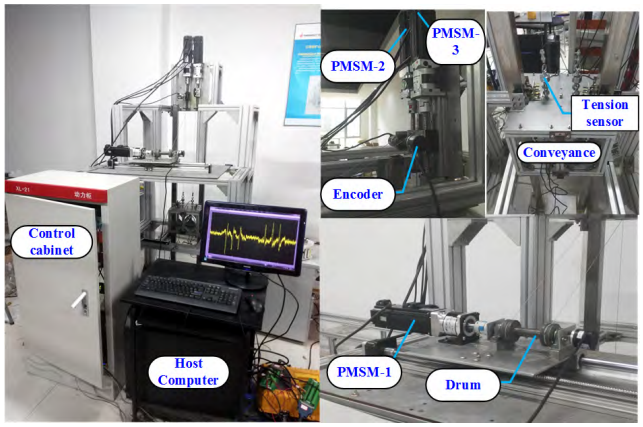

FIGURE 6. Photograph of the experimental apparatus.

TABLE 1. Parameters of the DRWMH experimental system.

Parameters	Values	Parameter	Values
r_{si}	0.03 m	$\theta_{qui}(i=1,2)$	45°
EA	10^6 N	r_{xc}	0.04 m
m_{sk}	3.57 kg	r_{yc}	0.1 m
ρ	0.004 kg/m	$y_{gyi}(i=1,2,3,4)$	0.118 m
$J_{si}(i=1,2)$	0.005 kg.m^2	L_d	2.8 mH
i_{wd}	10	L_q	2.8 mH
$i_{hsj}(j=1,2)$	10	p_n	4
ψ_f	0.32 Wb	J_{sk}	0.013 kg·m^2
$m_{vri}(i=1,2)$	0.01kg	$k_{vri}(i=1,2)$	1.8×10^5 N/m

A. DYNAMIC MODEL VERIFICATION OF THE DRWMH

To demonstrate that the above mathematical models are valid and can be used for controller design, the tension and tension difference signals of the two ropes in the absence of controller are collected and compared with the model simulation results as shown in Figure 7.

Figure 7(a) illustrates the reference evolution of the speed curve and its derivative to be followed by the conveyance. The reference speed curve contains two acceleration phases, two deceleration phases and two constant velocity phases, where the constant running speed is set to 0.09 m/s. With this kind of design, the conveyance will return to the initial position at the end of a test process, forming a repeating process. Figure 7(b) and Figure 7(c) present simulation and experimental comparison results of system tension and tension difference responses without control. It can be seen that simulation results and experimental results can achieve a good fit, which means that the proposed simplified model could predict system behavior and be used for analysis of controller performance.

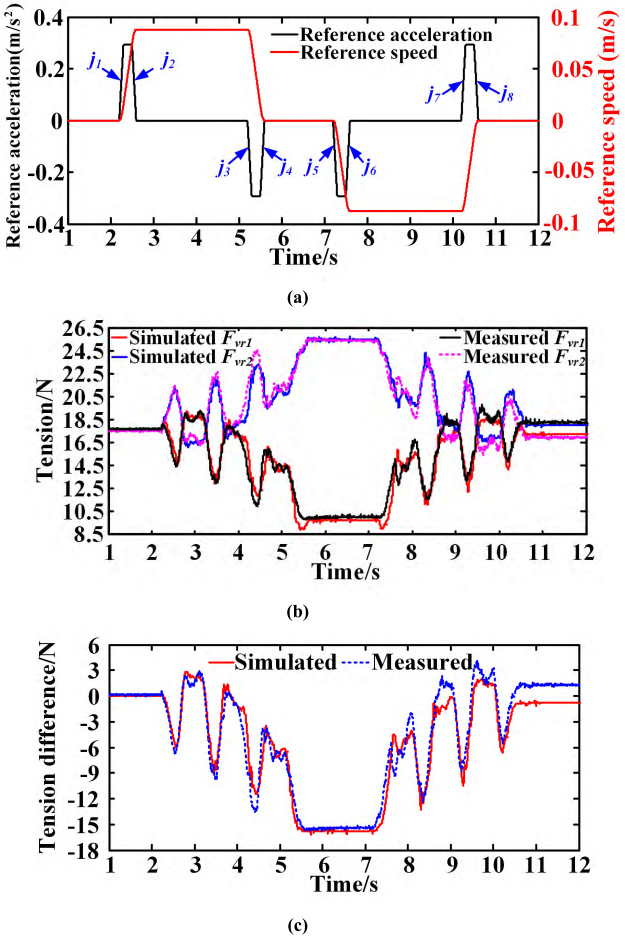

FIGURE 7. Reference curve and tension responses without control: (a) reference speed and acceleration curve; (b)tension responses; (c) tension difference.

B. EXPERIMENTAL RESULTS ANALYSIS

To demonstrate the effectiveness and superiority of the proposed hybrid adaptive learning fault-tolerant control algorithm, it is compared with traditional algorithms include PID controller and FFILC under normal and faults working conditions.

The control law of the classic PID controller [41] can be defined as

$$u(t) = K_p e(t) + K_i \int_0^t e(t)dt + K_d \dot{e}(t) \tag{43}$$

where K_p, K_i, K_d are respectively, the proportional and integral gains which are selected as follows: $K_p = 2.32$, $K_i = 0.02$, $K_d = 0.1$.

The control vector u generated from FFILC [42] can be obtained as

$$u_{k+1}(t) = K_{lp1} e_{k+1}(t) + K_{li1} \int_0^t e_{k+1}(t)dt + K_{ld1} \dot{e}_{k+1}(t) + u_{ff}(t) \tag{44}$$

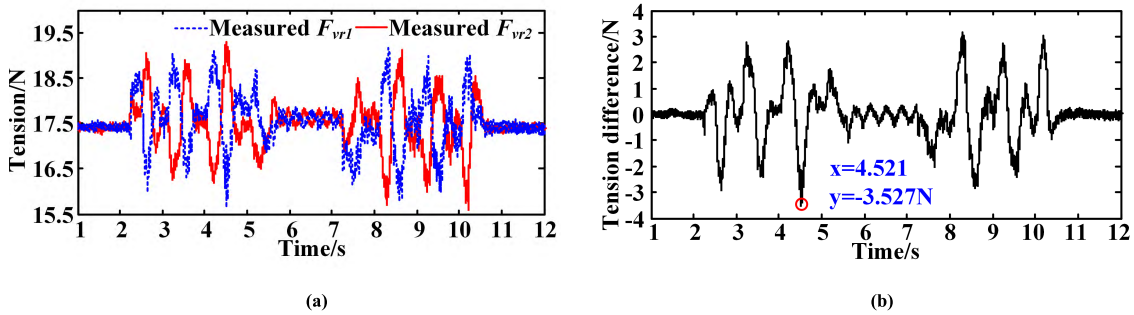

FIGURE 8. System responses with traditional PID control under no actuator faults conditions (Experimental): (a) tension responses; (b) tension difference.

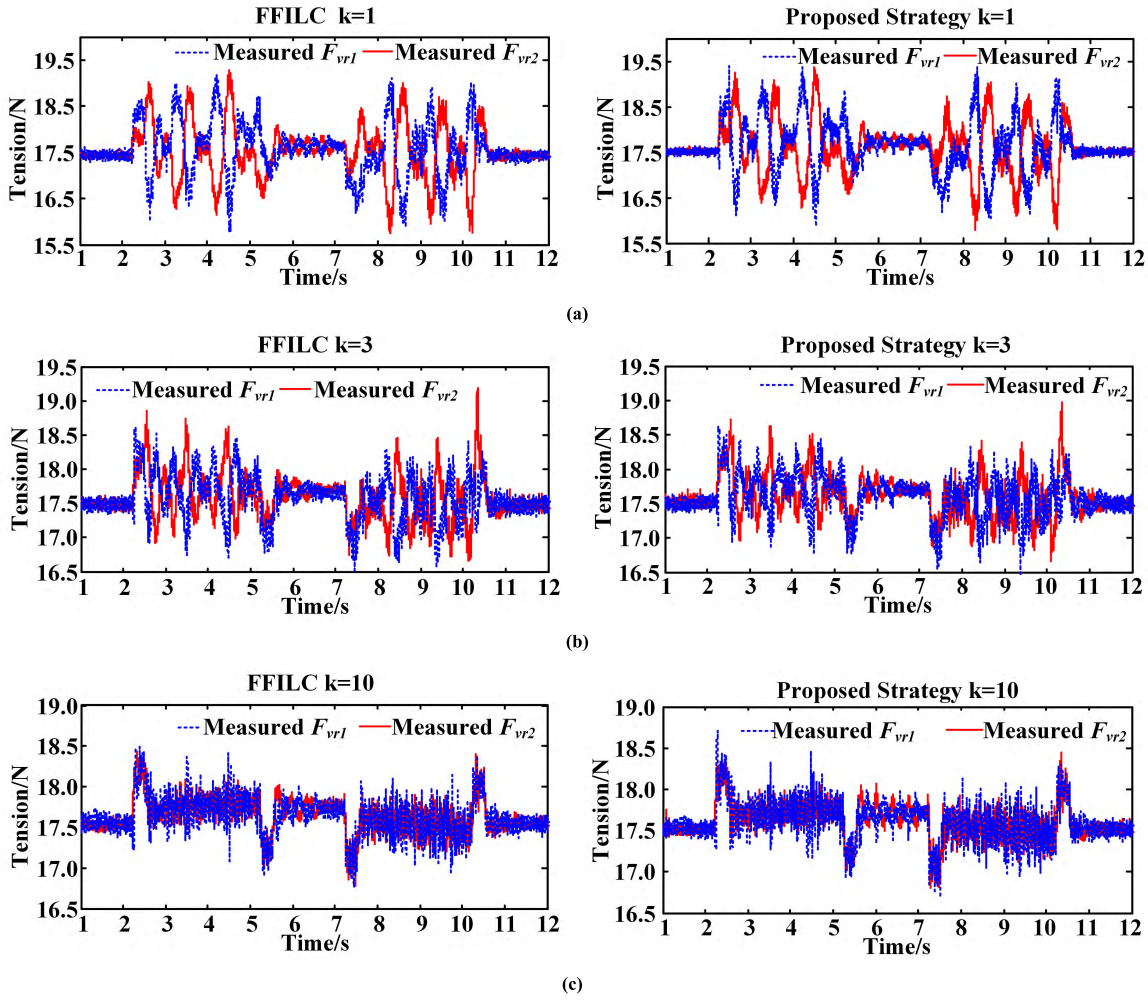

FIGURE 9. Tension responses with FFILC and proposed strategy under no actuator faults conditions (Experimental): (a) k = 1; (b) k = 3; (c) k = 10.

where $u_{ff}(t) = u_{ff}(t-T) + K_{lp2}e_k(t) + K_{ld2}\dot{e}_k(t)$. K_{lp1}, K_{li1}, K_{ld1} are respectively, the gains of the feedback parts which are chosen as 2.32, 0.02 and 0.1.$K_{lp2} = 0.5$ and $K_{ld2} = 0.01$ represent the gains of the feedforward part.

At the same time, set the parameters of the proposed control law (23) as follows: $\varpi_{pm} = 0.12, \kappa_{pm} = 0.01$, $\gamma_{pm} = 2.3$, $\lambda_{pm} = 0.02$.

Since the control objective of the system is to minimize the tension difference between the two ropes, the reference of the tension difference signal is set to 0. Here, two important indices maximum tension difference (MTD) and root-sum-square of absolute errors (RSSAE), are defined to evaluate the performances of all used controllers.

$$\text{MTD} = Max\left|\Delta F_{vr}^{k+1}(z)\right|, \quad z = 1\ldots N \tag{45}$$

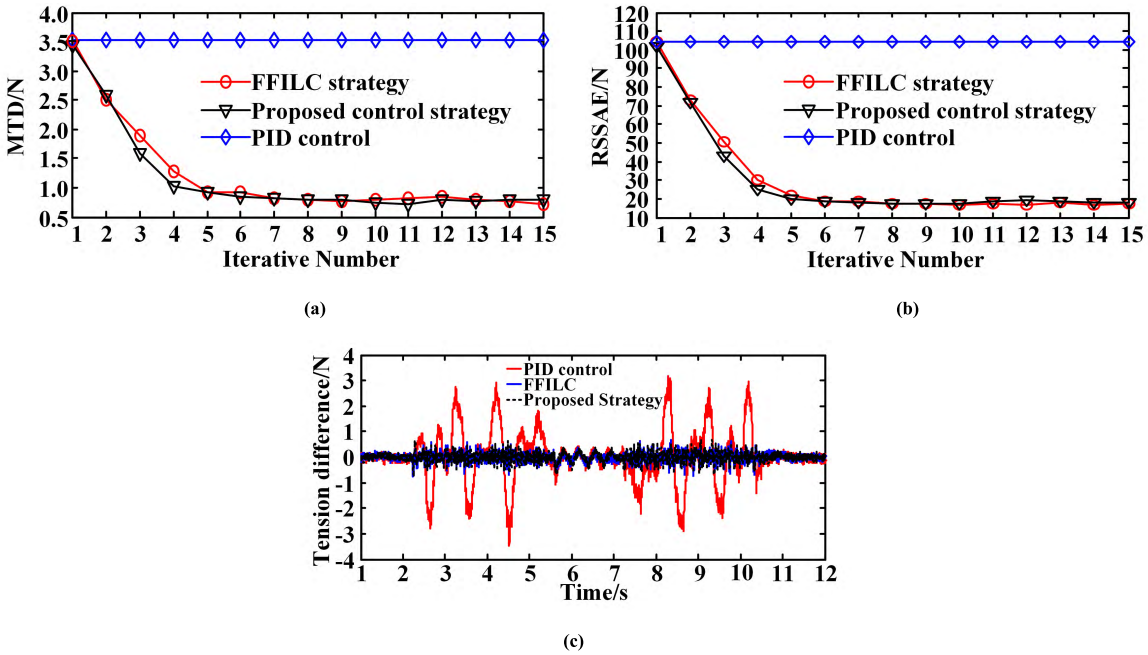

FIGURE 10. Tension difference and indices change with three controllers under no actuator faults conditions (Experimental): (a) MTD; (b) RSSAE; (c) tension difference.

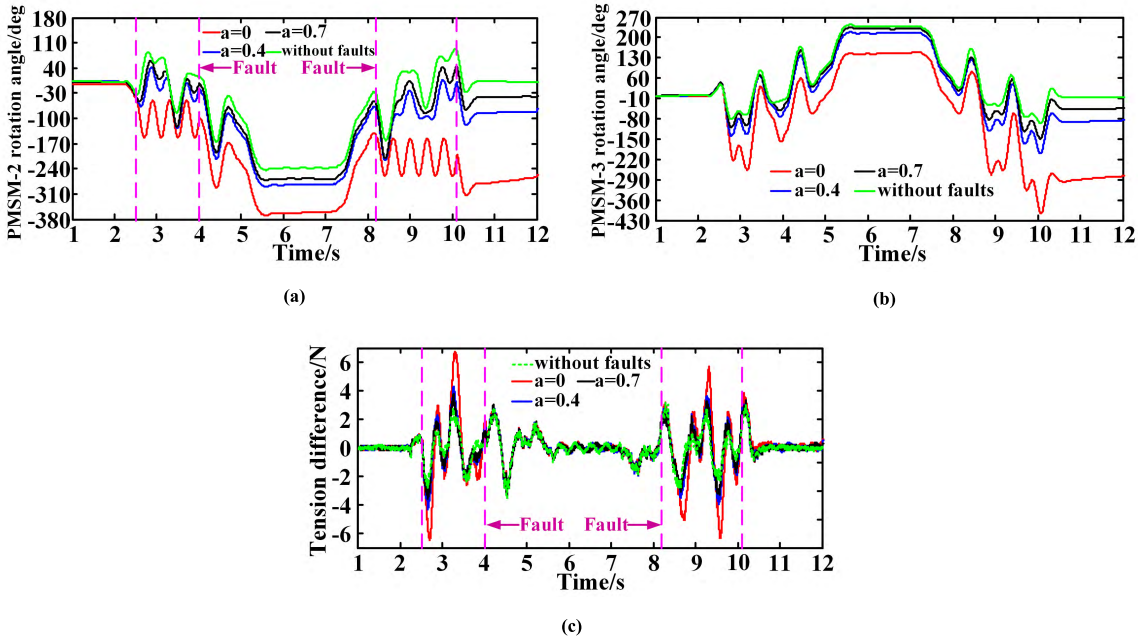

FIGURE 11. System responses with traditional PID control in the case of the second situation: (a) rotation angle of PMSM-2; (b) rotation angle of PMSM-3; (c) tension difference.

where $\Delta F_{vr}^{k+1}(z)$ represents the calculated tension difference signal during the $(k+1)$-th operation at z-th sampling point. The length of tension difference signals is denoted by N.

RSSAE indicates cumulative tension difference, which can be defined as

$$\text{RSSAE} = \sqrt{\left(\Delta F_{vr}^{k+1}(1)\right)^2 + \left(\Delta F_{vr}^{k+1}(2)\right)^2 + \cdots \left(\Delta F_{vr}^{k+1}(N)\right)^2} \tag{46}$$

Both indices are the smaller the better.

First, consider the case of no actuator faults, where only disturbances occur. The experimental results with above three controllers are shown in Figures 8-10. Figure 8 shows the tension responses of the experimental system with traditional PID control under no actuator faults conditions. Figure 9 illustrates tension responses of the experimental system under no actuator faults conditions with the FFILC and the proposed strategy. Figure 10 shows comparison results of MTD, RSSAE and tension difference

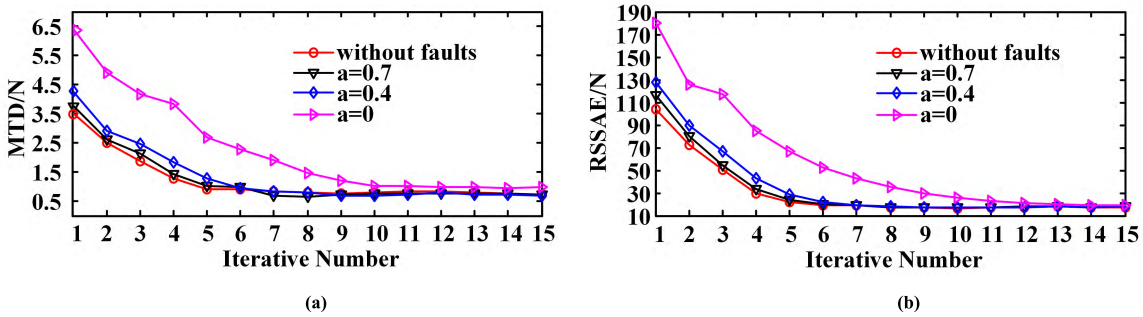

FIGURE 12. Indices change with FFILC in the case of the second situation: (Experimental): (a) MTD; (b) RSSAE.

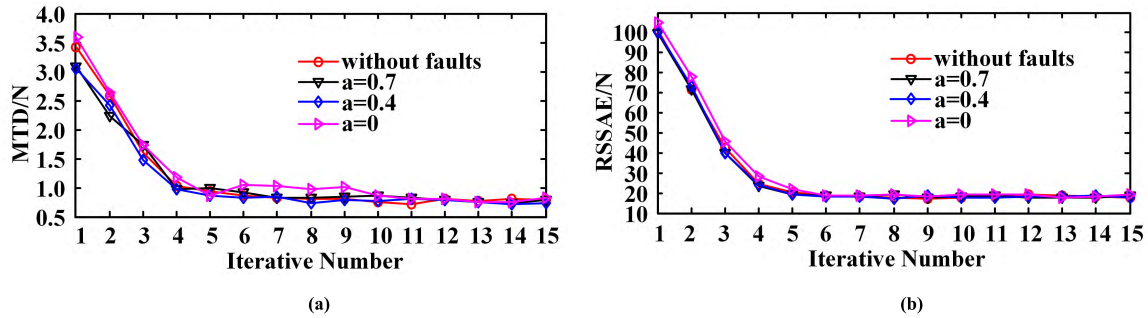

FIGURE 13. Indices change with proposed strategy in the case of the second situation: (Experimental): (a) MTD; (b) RSSAE.

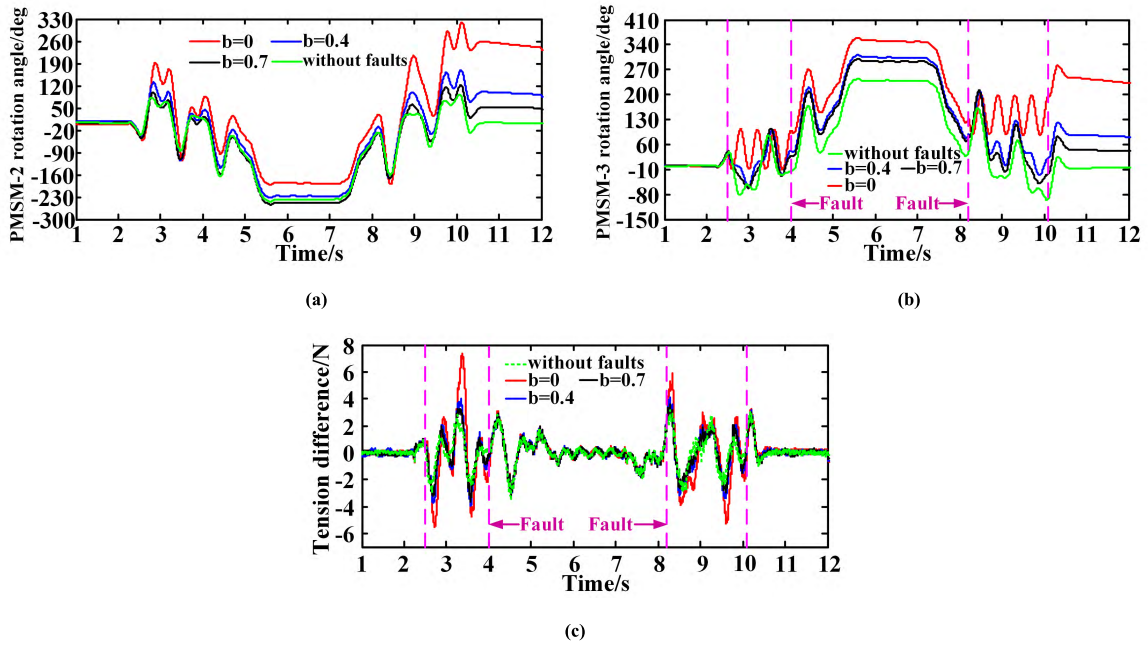

FIGURE 14. System responses with traditional PID control in the case of the third situation: (a) rotation angle of PMSM-2; (b) rotation angle of PMSM-3; (c) tension difference.

under no actuator faults conditions with above three controllers.

From the experimental results, it can be seen that traditional PID controller cannot suppress the tension difference fluctuation caused by external disturbances very well, the maximum tension difference reaches 3.572N. With designed parameters, as shown in Figure 9 and Figure 10, the MTD and RSSAE with both FFILC and the proposed controller gradually converge as the number of iterations increases. Values of MTD and RSSAE are consistently

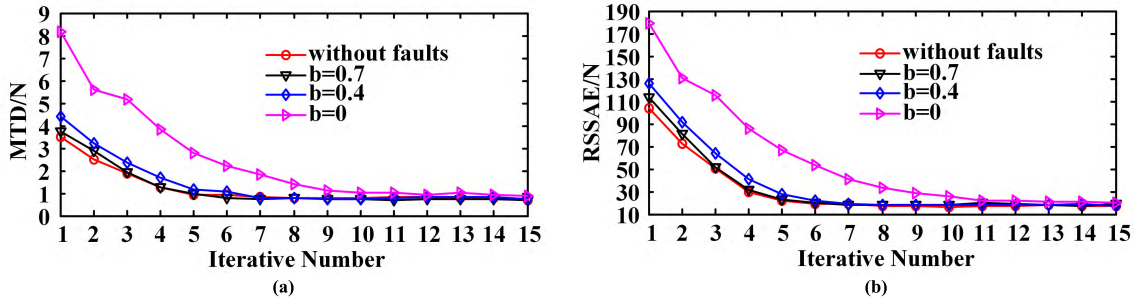

FIGURE 15. Indices change with FFILC in the case of the third situation: (Experimental): (a) MTD; (b) RSSAE.

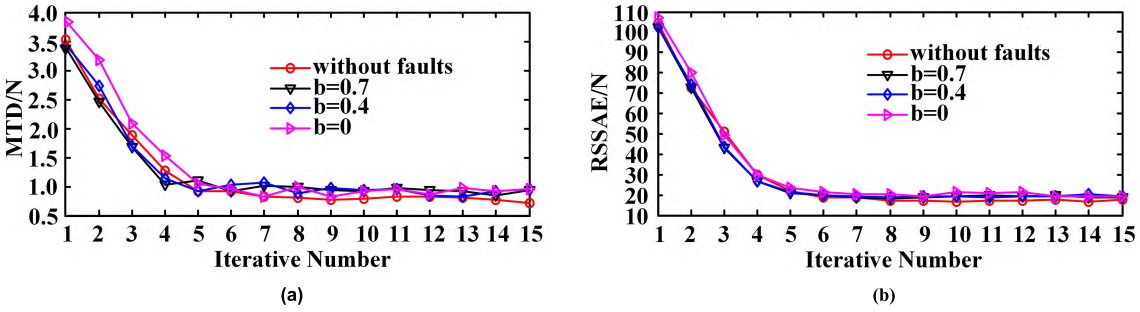

FIGURE 16. Indices change with proposed strategy in the case of the third situation: (Experimental): (a) MTD; (b) RSSAE.

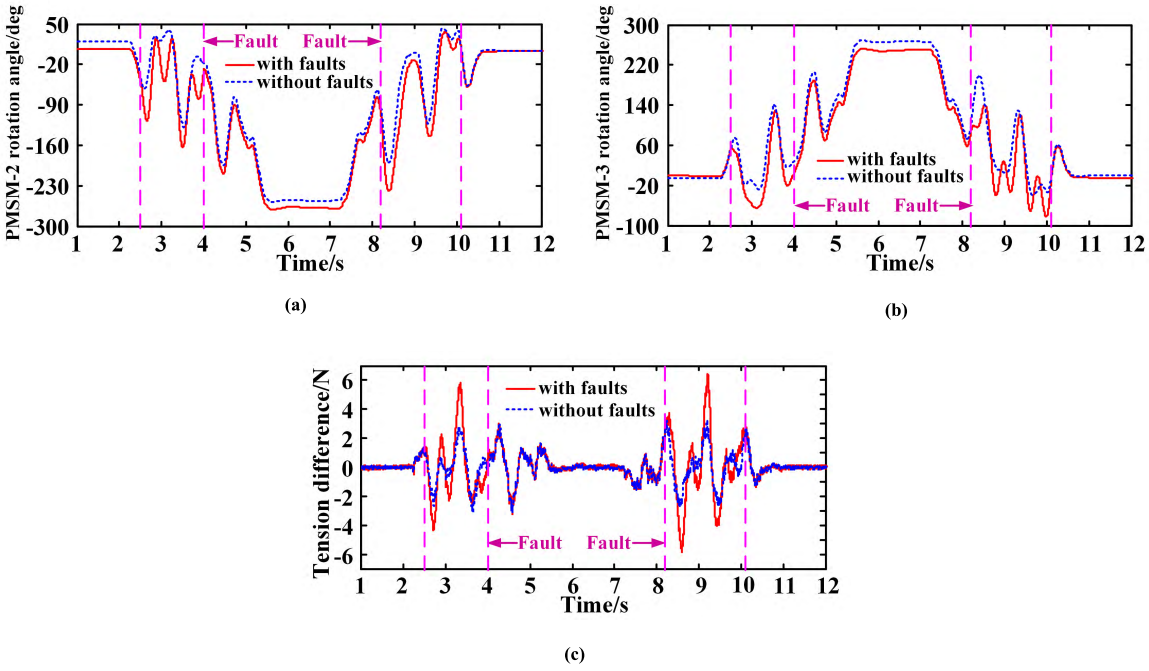

FIGURE 17. System responses with PID in the case of the fourth situation: (Experimental): (a) rotation angle of PMSM-2; (b) rotation angle of PMSM-3; (c) tension difference.

reduced up to fifth iteration and basically unchanged from fifth to fifteen iterations with both FFILC and the proposed strategy. Under no actuator faults conditions, the tension coordination control effect of the FFILC and the proposed strategy is basically the same.

In the second situation, consider the case of the left floating headgear sheave actuator failure. During conveyance rising process at time $t = 2.5$ s to time $t = 4$ s, and the devolution process at time $t = 8.2$ s to $t = 10.1$ s, the left movable headgear sheave suffers a loss of effective and an additive fault such as $u_1^f = au_1 + 0.1 \sin(t)$, where a is set to 0.7, 0.4, 0. The experimental results are shown in Figures 11-13. It can be seen that as degree of performance loss of the left actuator increases, the tension difference adjustment effect of the PID controller will become worse and worse, the convergence speed of the iterative learning controller will become slower

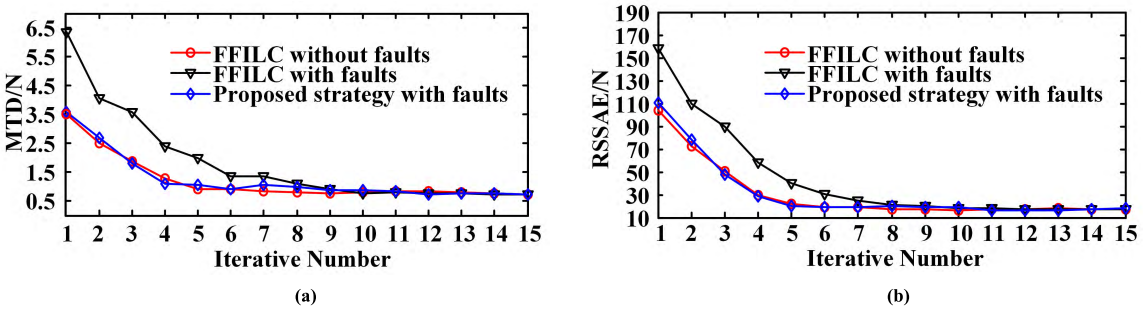

FIGURE 18. Indices change with FFILC and proposed strategy in the case of the fourth situation: (Experimental): (a) MTD; (b) RSSAE.

and slower. When the left actuator is completely disabled, the iterative learning controller will reach the tenth time to converge, while the proposed controller is able to maintain the same performance and convergence speed as in the case of no faults. Which demonstrates superiority and effectiveness of the proposed fault tolerant controller compared to the FFILC and the PID controller under actuator faults conditions.

In the third situation, consider the case of the right floating headgear sheave actuator failure. During conveyance rising process at time $t = 2.5$ s to time $t = 4$ s, and the devolution process at time $t = 8.2$ s to $t = 10.1$ s, the right movable headgear sheave suffers a loss of effective and an additive fault such as $u_2^f = bu_2 + 0.1\cos(t)$, where b is set to 0.7, 0.4, 0. The experimental results are shown in Figures 14-16. It can be seen that in the case of the right floating headgear sheave actuator failure, the proposed method is still more effective than PID controller and FFILC.

In the fourth situation, consider the simultaneous failure of both the left and right floating headgear sheave actuators. During conveyance rising process at time $t = 2.5$ s to time $t = 4$ s, the left movable headgear sheave fails according to the pattern $u_1^f = 0.4u_1 + 0.1\sin(t)$, the right movable headgear sheave undergoes fault defined as $u_2^f = 0.7u_2 + 0.1\cos(t)$. During conveyance devolution process at time $t = 8.2$ s to time $t = 10.1$ s, the left movable headgear sheave undergoes fault defined as $u_1^f = 0.7u_1 + 0.1\cos(t)$, the left movable headgear sheave fails according to the pattern $u_1^f = 0.4u_1 + 0.1\sin(t)$. The experimental results are shown in Figure 17 and Figure 18. It can be seen that even in the case where both actuators have the above failures, the proposed controller can maintain good performance of the system.

To this end, the effectiveness of the proposed fault-tolerant control method has been verified through experimental results under disturbances and actuator faults conditions.

VI. CONCLUSION

This paper carries an in-depth research on fault tolerant control of DRWMH under actuator faults and disturbances conditions. In order to overcome the impact of faults on the performance of traditional controllers and prevent major accident, in this paper, a novel strategy combining neural-based adaptive technique and iterative learning method is presented. The proposed control strategy adopts a multi-loop conformation, the inner of which employs a robust adaptive controller to deal with the faults of the movable headgear sheave, the outer iterative learning loop consists of a feed forward part and a feedback part to handle disturbances and residual fault influence. Theoretical analysis has been taken to show that the proposed control law is able to guarantee stability under fault conditions and can weaken the tension difference to a certain range. The proposed hybrid fault tolerant approach was successfully put into practice on a DRWMH experimental platform. Experimental results under multiple actuator faults conditions show that compared with the PID controller, the proposed controller has better control effects under the faults and disturbance conditions. Compared with FFILC, the proposed controller has faster convergence speed and can eliminate the impact of faults faster. In the future, we will study the fault-tolerant effect of the controller under time-delay conditions.

APPENDIX

PROOF OF THEOREM 2:

From (33), (34), (35), (38), we can get

$$M_{sk}\ddot{e}_{sk}^{k+1} + (C_{sk} + \rho_{sk}G_{sk}K_{skd1})\left(\dot{e}_{sk}^{k+1}\right) + \rho_{sk}G_{sk}K_{ski1}\int e_{sk} + \left(F_{sk} + \rho_{sk}G_{sk}K_{skp1}\right)\left(e_{sk}^{k+1}\right) = \bar{\tau}_{sk}^{k+1} \quad \text{(A1)}$$

where

$$\bar{\tau}_{sk}^{k+1} = M_{sk}\ddot{\theta}_{dsk} - P_{sk}\left(\theta_{dsk}, \dot{\theta}_{dsk}\right) - d_{sk} + O_{p_{gy}}(\bullet) - G_{sk}u_{ff}(t) \quad \text{(A2)}$$

(A1) can be reorganized as

$$M_{sk}\dot{\delta}_{sk}^{k+1} + (C_{sk} + \chi_{sk1})\left(\delta_{sk}^{k+1}\right) + \chi_{sk3}\left(e_{sk}^{k+1}\right) + \chi_{sk4}\int \delta_{sk}^{k+1} = \bar{\tau}_{sk}^{k+1} \quad \text{(A3)}$$

where

$$\chi_{sk1} = \rho_{sk}G_{sk}K_{skd1} - \varpi_{sk}M_{sk}, \quad \chi_{sk2} = \rho_{sk}G_{sk}K_{skp1} - \varpi_{sk}\chi_{sk1} - \frac{\rho_{sk}G_{sk}K_{ski1}}{\varpi_{sk}}$$

$$\chi_{sk3} = \chi_{sk2} + F_{sk} - \varpi_{sk}C_{sk}, \quad \chi_{sk4} = \frac{\rho_{sk}G_{sk}K_{ski1}}{\varpi_{sk}}, \quad \delta_{sk}^{k+1} = \dot{e}_{sk}^{k+1} + \varpi_{sk}e_{sk}^{k+1}.$$

Design a Lyapunov function as follows

$$V_{sk} = \frac{1}{2}M_{sk}\left(\delta_{sk}^{k}\right)^{2} + \frac{1}{2}\chi_{sk4}\left(\int_{0}^{t}\delta_{sk}^{k}d\tau\right)^{2} + \frac{1}{2}\chi_{sk2}\left(e_{sk}^{k}\right)^{2} + \frac{1}{2\rho_{sk}G_{sk}K_{skd2}}\int_{t-T}^{t}\bar{\tau}_{sk}^{2}d\tau \quad \text{(A4)}$$

The derivative of Lyapunov function with time can be given as

$$\dot{V}_{sk} = M_{sk}\delta_{sk}^{k}\dot{\delta}_{sk}^{k} + \chi_{sk4}\left(\int_{0}^{t}\delta_{sk}^{k}d\tau\right)\delta_{sk} + \chi_{sk2}e_{sk}^{k}\dot{e}_{sk}^{k} + \frac{1}{2\rho_{sk}G_{sk}K_{skd2}}\left[\left(\bar{\tau}_{sk}^{k+1}\right)^{2} - \left(\bar{\tau}_{sk}^{k}\right)^{2}\right] \quad \text{(A5)}$$

where $\bar{\tau}_{sk}^{k+1} = \bar{\tau}_{sk}(t)$, $\bar{\tau}_{sk}^{k} = \bar{\tau}_{sk}(t-T)$.

From (A3), (A5) can be represented as

$$\dot{V}_{sk} = -\left(C_{sk} + \chi_{sk1} - \frac{\rho_{sk}G_{sk}K_{skd2}}{2}\right)\left(\delta_{sk}^{k}\right)^{2} - \varpi_{sk}\chi_{sk3}\left(e_{sk}^{k}\right)^{2} + \frac{1}{2\rho_{sk}G_{sk}K_{skd2}}\pi_{sk} - e_{sk}^{k}\dot{e}_{sk}^{k}\left(F_{sk} - \varpi_{sk}C_{sk}\right) \quad \text{(A6)}$$

where

$$\pi_{sk} = \left(\bar{\tau}_{sk}^{k+1}\right)^{2} - \left(\bar{\tau}_{sk}^{k} - \rho_{sk}G_{sk}K_{skd2}\delta_{sk}^{k}\right)^{2} \quad \text{(A7)}$$

According to (A2), we have

$$\begin{aligned}\bar{\tau}_{sk}^{k+1} &= M_{sk}\ddot{\theta}_{skd} - P_{gy}\left(\theta_{dsk}, \dot{\theta}_{dsk}\right) - d_{sk} + O_{p_{gy}}(\bullet) \\ &\quad - G_{sk}\left[K_{skp2}\left(\varpi_{sk}e_{skf}^{k}(t) + \dot{e}_{skf}^{k}(t)\right) + u_{ff}(t-T)\right] \\ &= \bar{\tau}_{sk}^{k} - G_{sk}K_{skd2}\left(\varpi_{sk}e_{skf}^{k}(t) + \dot{e}_{skf}^{k}(t)\right) \\ &= \bar{\tau}_{sk}^{k} - \rho_{sk}G_{sk}K_{skd2}\delta_{sk}^{k} \end{aligned} \quad \text{(A8)}$$

Applying (A7) and (A8) to (A6), we get

$$\dot{V}_{sk} = -\left(C_{sk} + \chi_{sk1} - \frac{\rho_{sk}G_{sk}K_{skd2}}{2}\right)\left(\delta_{sk}^{k}\right)^{2} - \varpi_{sk}\chi_{sk3}\left(e_{sk}^{k}\right)^{2} - e_{sk}^{k}\dot{e}_{sk}^{k}\left(F_{sk} - \varpi_{sk}C_{sk}\right) \quad \text{(A9)}$$

(A9) can be reorganized as

$$\begin{aligned}\dot{V}_{sk} &= -\left(C_{sk} + \chi_{sk1} - \frac{\rho_{sk}G_{sk}K_{skd2}}{2}\right)\left(\dot{e}_{sk}^{k}\right)^{2} \\ &\quad - \left(C_{sk} + \chi_{sk1} - \frac{\rho_{sk}G_{sk}K_{skd2}}{2}\right)\left(\varpi_{sk}e_{sk}^{k}\right)^{2} \\ &\quad + \left(\frac{\rho_{sk}G_{sk}K_{skd2}}{2} - C_{sk} - \chi_{sk1}\right)\left(2\varpi_{sk}\dot{e}_{sk}^{k}e_{sk}^{k}\right) \\ &\quad + e_{sk}^{k}\dot{e}_{sk}^{k}\left(\varpi_{sk}C_{sk} - F_{sk}\right) - \varpi_{sk}\chi_{sk3}\left(e_{sk}^{k}\right)^{2} \end{aligned} \quad \text{(A10)}$$

From (40), (41), (42), we can get

$$\dot{V}_{sk} \le -\phi_{ska}\left|\dot{e}_{sk}^{k}\right|^{2} + \left|e_{sk}^{k}\right|\left|\dot{e}_{sk}^{k}\right|\zeta_{sk} - \varpi_{sk}\phi_{skb}\left|e_{sk}^{k}\right|^{2} + 2\varpi_{sk}\phi_{ska}\left|\dot{e}_{sk}^{k}\right|\left|e_{sk}^{k}\right| \quad \text{(A11)}$$

(A11) can be reorganized as

$$\dot{V}_{sk} \le -\frac{1}{2}\varpi_{sk}\left[\phi_{skb} - \frac{1}{\varpi_{sk}\phi_{ska}}\left(\varpi_{sk}\phi_{ska} + \frac{\zeta_{sk}}{2}\right)^{2}\right]\left|e_{sk}^{k}\right|^{2} - \frac{1}{2}\left[\phi_{ska} - \frac{1}{\varpi_{sk}\phi_{skb}}\left(\varpi_{sk}\phi_{ska} + \frac{\zeta_{sk}}{2}\right)^{2}\right]\left|\dot{e}_{sk}^{k}\right|^{2} \quad \text{(A12)}$$

According to (39), we have

$$\psi_{ska} = \phi_{ska} - \frac{1}{\varpi_{sk}\phi_{skb}}\left(\varpi_{sk}\phi_{ska} + \frac{\zeta_{sk}}{2}\right)^{2} \ge 0 \quad \text{(A13)}$$

$$\psi_{skb} = \phi_{skb} - \frac{1}{\varpi_{sk}\phi_{ska}}\left(\varpi_{sk}\phi_{ska} + \frac{\zeta_{sk}}{2}\right)^{2} \ge 0 \quad \text{(A14)}$$

Applying (A13) and (A14) to (A12), we get

$$\dot{V}_{sk} \le -\frac{1}{2}\varpi_{sk}\psi_{skb}\left|e_{sk}^{k}\right|^{2} - \frac{1}{2}\psi_{ska}\left|\dot{e}_{sk}^{k}\right|^{2} \le 0 \quad \text{(A15)}$$

Thence, we prove Theorem 2.

ACKNOWLEDGMENT

The authors would like to thank the editors, associate editors, and anonymous reviewers for their constructive comments.

REFERENCES

[1] S. Kaczmarczyk and W. Ostachowicz, "Transient vibration phenomena in deep mine hoisting cables. Part 2: Numerical simulation of the dynamic response," *J. Sound Vibrat.*, vol. 262, no. 2, pp. 245–289, Apr. 2003. doi: 10.1016/S0022-460X(02)01148-3.

[2] X. Peng, X.-S. Gong, and J.-J. Liu, "The study on crossover layouts of multi-layer winding grooves in deep mine hoists based on transverse vibration characteristics of catenary rope," *Proc. Inst. Mech. Eng. I, J. Syst. Control Eng.*, vol. 233, no. 2, pp. 118–132, Feb. 2018. doi: 10.1177/0959651818785309.

[3] X.-D. Chang *et al.*, "Breaking failure analysis and finite element simulation of wear-out winding hoist wire rope," *Eng. Failure Anal.*, vol. 95, pp. 1–17, Jan. 2019. doi: 10.1016/j.engfailanal.2018.08.027.

[4] X. Li, Z.-C. Zhu, and G. Shen, "A switching-type controller for wire rope tension coordination of electro-hydraulic-controlled double-rope winding hoisting systems," *Proc. Inst. Mech. Eng. I, J. Syst. Control Eng.*, vol. 230, no. 10, pp. 1126–1144, Nov. 2016. doi: 10.1177/0959651816672787.

[5] J. Wang, Y. Pi, Y. Hu, and X. Gong, "Modeling and dynamic behavior analysis of a coupled multi-cable double drum winding hoister with flexible guides," *Mech. Mach. Theory*, vol. 108, pp. 191–208, Feb. 2017. doi: 10.1016/j.mechmachtheory.2016.10.021.

[6] B. Zi, B. Y. Duan, J. L. Du, and H. Bao, "Dynamic modeling and active control of a cable-suspended parallel robot," *Mechatronics*, vol. 18, no. 1, pp. 1–12, Feb. 2008. doi: 10.1016/j.mechatronics.2007.09.004.

[7] Z.-C. Zhu, X. Li, G. Shen, and W.-D. Zhu, "Wire rope tension control of hoisting systems using a robust nonlinear adaptive backstepping control scheme," *ISA Trans.*, vol. 72, pp. 256–272, Jan. 2018. doi: 10.1016/j.isatra.2017.11.007.

[8] J. Wang, Y. Pi, and M. Krstic, "Balancing and suppression of oscillations of tension and cage in dual-cable mining elevators," *Automatica*, vol. 98, pp. 223–238, Dec. 2018. doi: 10.1016/j.automatica.2018.09.027.

[9] T. Wang, S. Tong, J. Yi, and H. Li, "Adaptive inverse control of cable-driven parallel system based on type-2 fuzzy logic systems," *IEEE Trans. Fuzzy Syst.*, vol. 23, no. 5, pp. 1803–1816, Oct. 2015. doi: 10.1109/TFUZZ.2014.2379284.

[10] M. A. Khosravi and H. D. Taghirad, "Robust PID control of fully-constrained cable driven parallel robots," *Mechatronics*, vol. 24, no. 2, pp. 87–97, Mar. 2014. doi: 10.1016/j.mechatronics.2013.12.001.

[11] S. Yin, H. Gao, J. Qiu, and O. Kaynak, "Descriptor reduced-order sliding mode observers design for switched systems with sensor and actuator faults," *Automatica*, vol. 76, pp. 282–292, Feb. 2017. doi: 10.1016/j.automatica.2016.10.025.

[12] J. Niu, F. Chen, and G. Tao, "Nonlinear fuzzy fault-tolerant control of hypersonic flight vehicle with parametric uncertainty and actuator fault," *Nonlinear Dyn*, vol. 92, no. 3, pp. 1299–1315, May 2018. doi: 10.1007/s11071-018-4127-z.
[13] H. A. Talebi, K. Khorasani, and S. Tafazoli, "A recurrent neural-network-based sensor and actuator fault detection and isolation for nonlinear systems with application to the satellite's attitude control subsystem," *IEEE Trans. Neural Netw.*, vol. 20, no. 1, pp. 45–60, Jan. 2009. doi: 10.1109/TNN.2008.2004373.
[14] Y. Wang, J. Shi, D. Zhou, and F. Gao, "Iterative learning fault-tolerant control for batch processes," *Ind. Eng. Chem. Res.*, vol. 45, no. 26, pp. 9050–9060, Dec. 2006. doi: 10.1021/ie060726p.
[15] J. Jiang and X. Yu, "Fault-tolerant control systems: A comparative study between active and passive approaches," *Annu. Rev. Control*, vol. 36, no. 1, pp. 60–72, Apr. 2012. doi: 10.1016/j.arcontrol.2012.03.005.
[16] S. Yin, B. Xiao, S. X. Ding, and D. Zhou, "A review on recent development of spacecraft attitude fault tolerant control system," *IEEE Trans. Ind. Electron.*, vol. 63, no. 5, pp. 3311–3320, May 2016. doi: 10.1109/TIE.2016.2530789.
[17] A.-R. Merheb, H. Noura, and F. Bateman, "Design of passive fault-tolerant controllers of a quadrotor based on sliding mode theory," *Int. J. Appl. Math. Comput. Sci.*, vol. 25, no. 3, pp. 561–576, Sep. 2015. doi: 10.1515/amcs-2015-0042.
[18] R. Wang, H. Jing, H. R. Karimi, and N. Chen, "Robust fault-tolerant H∞ control of active suspension systems with finite-frequency constraint," *Mech. Syst. Signal Process.*, vols. 62–63, pp. 341–355, Oct. 2015. doi: doi.org/10.1016/j.ymssp.2015.01.015.
[19] P. Yazdjerdi and N. Meskin, "Design and real-time implementation of actuator fault-tolerant control for differential-drive mobile robots based on multiple-model approach," *Proc. Inst. Mech. Eng. I, J. Syst. Control Eng.*, vol. 232, no. 6, pp. 652–661, Jul. 2018. doi: 10.1177/0959651818779849.
[20] Q. Shen, B. Jiang, and V. Cocquempot, "Adaptive fuzzy observer-based active fault-tolerant dynamic surface control for a class of nonlinear systems with actuator faults," *IEEE Trans. Fuzzy Syst.*, vol. 22, no. 2, pp. 338–349, Apr. 2014. doi: 10.1109/TFUZZ.2013.2254493.
[21] Z. Gao, P. Cheng, M. Qian, G. Jiang, and J. Lin, "Active fault-tolerant control approach design for rigid spacecraft with multiple actuator faults," *Proc. Inst. Mech. Eng. I, J. Syst. Control Eng.*, vol. 232, no. 10, pp. 1365–1378, Nov. 2018. doi: 10.1177/0959651818782847.
[22] G. Tao, "Direct adaptive actuator failure compensation control: A tutorial," *J. Control Decision*, vol. 1, no. 1, pp. 75–101, Jan. 2014. doi: 10.1080/23307706.2014.885292.
[23] Z. Mao, G. Tao, B. Jiang, and X.-G. Yan, "Adaptive actuator compensation of position tracking for high-speed trains with disturbances," *IEEE Trans. Veh. Technol.*, vol. 67, no. 7, pp. 5706–5717, Jul. 2018. doi: 10.1109/TVT.2018.2808360.
[24] S. Boulouma, S. Labiod, and H. Boubertakh, "Direct adaptive control of a flexible spacecraft with disturbances and uncertain actuator failures," *Mech. Syst. Signal Process.*, vol. 110, pp. 73–89, Sep. 2018. doi: 10.1016/j.ymssp.2018.03.007.
[25] M. Van, S. S. Ge, and H. Ren, "Robust fault-tolerant control for a class of second-order nonlinear systems using an adaptive third-order sliding mode control," *IEEE Trans. Syst., Man, Cybern. Syst.*, vol. 47, no. 2, pp. 221–228, Feb. 2017. doi: 10.1109/TSMC.2016.2557220.
[26] Y. Ma, B. Jiang, G. Tao, and Y. Cheng, "A direct adaptive actuator failure compensation scheme for satellite attitude control systems," *Proc. Inst. Mech. Eng., G, J. Aerosp. Eng.*, vol. 228, no. 4, pp. 542–556, Mar. 2014. doi: 10.1177/0954410013476191.
[27] X. Peng, X.-S. Gong, and J.-J. Liu, "Vibration control on multilayer cable moving through the crossover zones on mine hoist," *Shock Vib.*, vol. 2016, May 2016, Art. no. 6878021. doi: 10.1155/2016/6878021.
[28] S. Kaczmarczyk and W. Ostachowicz, "Transient vibration phenomena in deep mine hoisting cables. Part 1: Mathematical model," *J. Sound Vibrat.*, vol. 262, no. 2, pp. 219–244, Apr. 2003. doi: 10.1016/S0022-460X(02)01137-9.
[29] J. Yao, X. Xiao, A. Peng, Y. Jiang, and C. Ma, "Assessment of safety for axial fluctuations of head sheaves in mine hoist based on coupled dynamic model," *Eng. Failure Anal.*, vol. 51, pp. 98–107, May 2015. doi: 10.1016/j.engfailanal.2015.02.011.
[30] X. Arrasate, S. Kaczmarczyk, G. Almandoz, J. M. Abete, and I. Isasa, "The modelling, simulation and experimental testing of the dynamic responses of an elevator system," *Mech. Syst. Signal Process.*, vol. 42, nos. 1–2, pp. 258–282, Jan. 2014. doi: 10.1016/j.ymssp.2013.05.021.
[31] B. Li and X. Rui, "Vibration control of uncertain multiple launch rocket system using radial basis function neural network," *Mech. Syst. Signal Process.*, vol. 98, pp. 702–721, Jan. 2018. doi: 10.1016/j.ymssp.2017.05.036.
[32] Y. Wang, F. Gao, and F. J. Doyle, "Survey on iterative learning control, repetitive control, and run-to-run control," *J. Process Control*, vol. 19, no. 10, pp. 1589–1600, Dec. 2009. doi: 10.1016/j.jprocont.2009.09.006.
[33] A. Tayebi, "Adaptive iterative learning control for robot manipulators," *Automatica*, vol. 40, no. 7, pp. 1195–1203, Jul. 2004. doi: 10.1016/j.automatica.2004.01.026.
[34] Q. Yu, Z. Hou, and J.-X. Xu, "D-type ILC based dynamic modeling and norm optimal ILC for high-speed trains," *IEEE Trans. Control Syst. Technol.*, vol. 26, no. 2, pp. 652–663, Mar. 2018. doi: 10.1109/TCST.2017.2692730.
[35] L. Wang, F. Liu, J. Yu, P. Li, R. Zhang, and F. Gao, "Iterative learning fault-tolerant control for injection molding processes against actuator faults," *J. Process Control*, vol. 59, pp. 59–72, Nov. 2017. doi: 10.1016/j.jprocont.2017.08.013.
[36] A. Mohammadpour, S. Mishra, and L. Parsa, "Fault-tolerant operation of multiphase permanent-magnet machines using iterative learning control," *IEEE J. Emerg. Sel. Topics Power Electron.*, vol. 2, no. 2, pp. 201–211, Jun. 2014. doi: 10.1109/JESTPE.2013.2295537.
[37] S. Qian, B. Zi, and H. Ding, "Dynamics and trajectory tracking control of cooperative multiple mobile cranes," *Nonlinear Dyn.*, vol. 83, nos. 1–2, pp. 89–108, Jan. 2016. doi: 10.1007/s11071-015-2313-9.
[38] X. Chen, Z. Zhu, G. Shen, and W. Li, "Tension coordination control of double-rope winding hoisting system using hybrid learning control scheme," *Proc. Inst. Mech. Eng. I, J. Syst. Control Eng.*, Jan. 2019, Art. no. 0959651818824009. doi: 10.1177/0959651818824009.
[39] Z. Zhou, B. Zhang, and D. Mao, "Robust sliding mode control of PMSM based on rapid nonlinear tracking differentiator and disturbance observer," *Sensors*, vol. 18, no. 4, p. 1031, Mar. 2018. doi: 10.3390/s18041031.
[40] T.-Y. Kuc and W.-G. Han, "An adaptive PID learning control of robot manipulators," *Automatica*, vol. 36, no. 5, pp. 717–725, May 2000. doi: 10.1016/S0005-1098(99)00198-3.
[41] H. Feng *et al.*, "Robotic excavator trajectory control using an improved GA based PID controller," *Mech. Syst. Signal Process.*, vol. 105, pp. 153–168, May 2018. doi: 10.1016/j.ymssp.2017.12.014.
[42] A. Madady, "An extended PID type iterative learning control," *Int. J. Control, Autom. Syst.*, vol. 11, no. 3, pp. 470–481, Jun. 2013. doi: 10.1007/s12555-012-0350-4.

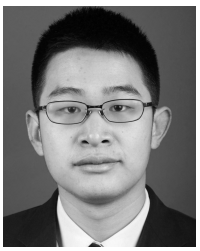

XIAO CHEN received the B.E. and M.E. degrees from the School of Mechatronic Engineering, China University of Mining and Technology, Xuzhou, China, in 2014 and 2016, respectively, where he is currently pursuing the Ph.D. degree in mechatronic engineering.

His current research interests include fault tolerant control, fault diagnosis, and remaining useful life prediction.

ZHEN-CAI ZHU received the Ph.D. degree from the China University of Mining and Technology, Xuzhou, China, in 2000. He joined Central South University, Changsha, China, as a Postdoctoral Researcher, in 2001. He was a Visiting Research Scholar with the University of Wuppertal, Germany, from 2010 to 2011. He is currently a Professor of mechanical engineering with the School of Mechatronic Engineering, China University of Mining and Technology, where he is also the Dean of the Academy of Science and Technology. His current research interests are mechanical system reliability, condition monitoring, fault diagnosis, and remaining useful life prediction.

WEI LI received the M.E. and Ph.D. degrees from the University of Duisburg-Essen, Duisburg, Germany, in 2006 and 2009, respectively. He is currently a Professor of mechatronic engineering with the School of Mechatronic Engineering, China University of Mining and Technology, Xuzhou, China. His current research interests include condition monitoring, fault diagnosis, and remaining useful life prediction of rotating machinery.

GANG SHEN received the B.S. degree from Jiamusi University, in 2005, and the M.S. and Ph.D. degrees from the Harbin Institute of Technology, in 2007 and 2011, respectively. He is currently a Professor with the School of Mechanical and Electrical Engineering, China University of Mining and Technology. His research interests include electro-hydraulic servo control, parallel robot, and loading systems.